magnetochemistry

MDPI

Article

The Solid Solutions $(Per)_2[Pt_xAu_{(1-x)}(mnt)_2]$; Alloying Para- and Diamagnetic Anions in Two-Chain Compounds

Manuel Matos [1,2], Gregoire Bonfait [3,4], Isabel C. Santos [3], Mónica L. Afonso [3], Rui T. Henriques [1] and Manuel Almeida [3,*]

1 Instituto de Telecomunicações, P-1049-001 Lisboa, Portugal; mmatos@deq.isel.pt (M.M.); rui.henriques@lx.it.pt (R.T.H.)
2 Chemical Engineering Department, ISEL, P-1959-007 Lisboa, Portugal
3 C^{2}TN-Centro de Ciências e Tecnologias Nucleares, Instituto Superior Técnico, Universidade de Lisboa, P-2695-066 Bobadela LRS, Portugal; gb@fct.unl.pt (G.B.); icsantos@ctn.tecnico.ulisboa.pt (I.C.S.); mochaves@sapo.pt (M.L.A.)
4 Physics Department, Faculty of Sciences and Technologies, Universidade Nova de Lisboa, P-2829-516 Caparica, Portugal
* Correspondence: malmeida@ctn.tecnico.ulisboa.pt; Tel.: +351-219-946-171

Academic Editor: Carlos J. Gómez García
Received: 28 April 2017; Accepted: 26 May 2017; Published: 13 June 2017

Abstract: The α-$(Per)_2[M(mnt)_2]$ compounds with M = Pt and Au are isostructural two-chain solids that in addition to partially oxidized conducting perylene chains also contain anionic chains that can be either paramagnetic in the case of M = Pt or diamagnetic for M = Au. The electrical transport and magnetic properties of the solid solutions $(Per)_2[Pt_x\text{-}Au_{(1-x)}(mnt)_2]$ were investigated. The incorporation of paramagnetic $[Pt(mnt)_2]$ impurities in the diamagnetic chains, and the effect of breaking the paramagnetic chains with diamagnetic centers for the low and high Pt range of concentrations were respectively probed. In the low Pt concentration range, there is a fast decrease of the metal-to-insulator transition from 12.4 K in the pure Au compound to 9.7 K for $x = 0.1$ comparable to the 8.1 K in the pure Pt compound. In the range $x = 0.50-0.95$, only β-phase crystals could be obtained. The spin-Peierls transition of the pure Pt compound, simultaneous with metal-to-insulator (Peierls) transition is still present for 2% of diamagnetic impurities ($x = 0.98$) with transition temperature barely affected. Single crystal X-ray diffraction data obtained a high-quality structural refinement of the α-phase of the Au and Pt compounds. The β-phase structure was found to be composed of ordered layers with segregated donors and anion stacks, which alternate with disordered layers. The semiconducting properties of the β-phase are due to the disorder localization effects.

Keywords: organic conductors; perylene; metal-dithiolate; organic alloys; conductivity; thermoelectric power; magnetic susceptibility; spin-Peierls transition; Peierls transition

1. Introduction

The charge transfer salts from the organic aromatic electron donor perylene (Per) and monoanionic transition metal bis-maleonitriledithiolate complexes $[M(mnt)_2]$ (M = Au, Pt, Pd Cu, Ni Fe and Co), (Scheme 1) with general formula $(Per)_2[M(mnt)_2]$, constitute a large family of compounds that since the first seminal paper in 1974 [1,2], have been the topic of a large number of successive studies and the subject of a few reviews [3–5], including a recent one focused on structural Peierls and spin-Peierls inabilities in this issue [6]. These studies soon provided evidence that these compounds can be obtained in two polymorphs, α- and β- [7]. The α-phases, with highly conducting quasi-1D metallic properties at higher temperatures, are particularly interesting since after more than 40 years of developments in the field of

molecular conductors, they remain a unique family of compounds with two types of chains (magnetic and conducting). The β-phases present a less interesting semiconducting behavior, which is associated with a so far poorly resolved disordered structure. In spite of many efforts and several studies, the conditions that favor the formation of any of these two polymorphic phases have remained uncontrolled, but often electrocrystallization batches are entirely composed of only one of the polymorphs.

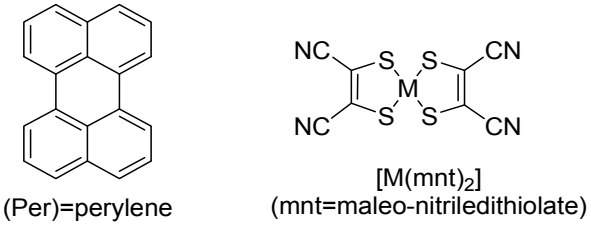

Scheme 1. Molecular structure of perylene and $[M(mnt)_2]$.

The main feature of the α-phases is that conducting and magnetic chains can exist side by side in the same structure and in mutual interaction. The conducting chains in these compounds are provided by regular stacks of partially oxidized perylene molecules $(Per)^{1/2+}$ which behave as a ¾-filled 1D electron band system. The square planar anionic complexes $[M(mnt)_2]^-$ are also stacked alongside and in between the donor stacks (see Section 2.1). For some metals (e.g., M = Ni, Pd, Pt), the anions have a localized $S = 1/2$ magnetic moment, while in other metals such as Au and Cu the anions are diamagnetic. The interaction between these two types of chains and the competition between the instabilities of these 1D magnetic and conducting systems is a unique feature of this family of compounds that has been the central point of discussion in different studies.

Among the different members of this family, the pair of better-characterized compounds with neighbor transition metals in the periodic table, Au and Pt, where the anionic chains are respectively diamagnetic and paramagnetic, are special members which through comparison can establish evidence for the role of the paramagnetic chains in the properties of these compounds. Both compounds present a metal-to-insulator transition at 8 K and 12 K respectively that has been ascribed to a Peierls distortion (tetramerisation) of the perylene chains, which in a first approach behave as a ¾-filled band system. The Pt compound presents, in addition to the Peierls transition involving the conducting perylene chains, a spin-Peierls transition at the same critical temperature that corresponds to a dimerization of the spin-carrying units $[Pt(mnt)_2]^-$. The structural aspects of these transitions were the subject of a detailed review in this Special Issue of *Magnetochemistry* [6].

In this paper, we present results of a detailed study of the electrical transport and magnetic properties of the solid solutions $(Per)_2[Pt_x\text{-}Au_{(1-x)}(mnt)_2]$, for which some preliminary results were previously reported [8,9]. This study illustrated for the α-phases both the effect of incorporating paramagnetic impurities in the diamagnetic anionic chains and the breaking effect of diamagnetic centers in the paramagnetic anionic chains for the low and high Pt range of concentrations, respectively. In the range $x = 0.50-0.95$, only β-phase crystals could be grown and a partial description of the crystal structure of this disordered phase was obtained.

2. Results and Discussion

Single crystals with the composition $(Per)_2[Pt_x\text{-}Au_{(1-x)}(mnt)_2]$ in the entire composition range $x = 0-1$ were obtained by electrocrystallization from dichloromethane solutions of perylene and variable relative amounts of the gold and platinum complexes, under general galvanostatic conditions, as previously described for the pure compounds [10,11]. The quality and shape of the crystals was found; however, it was variable and dependent on the composition x. For x in the range 0.0–0.4 and 0.98–1.0, larger needle or elongated plate-shaped crystals could be obtained, with the largest ones reaching $10 \times 0.5 \times 0.08$ mm^3 for the pure Pt and Au compounds. However, in the range $x = 0.5-0.95$,

only very small needle-shaped crystals could be obtained, which as described below, were all found to pertain to the β-phase polymorph.

The Scanning Electron Microscopy–Energy Dispersive Spectroscopy (SEM–EDS) microanalysis of the different crystals obtained in all composition ranges (Figure 1) revealed that the relative Pt and Au concentrations in the crystals closely follow those of the solution, denoting the formation of Au–Pt solid solutions in the full range of compositions, as expected in view of the similar size of the Pt and Au atoms and close similarities of the two isostructural compounds with identical lattice parameters [10,12]. However, as seen in Figure 1, there is a small deviation of the crystal composition from that of the solution, in the sense that the crystals tend to slightly enrich in Pt.

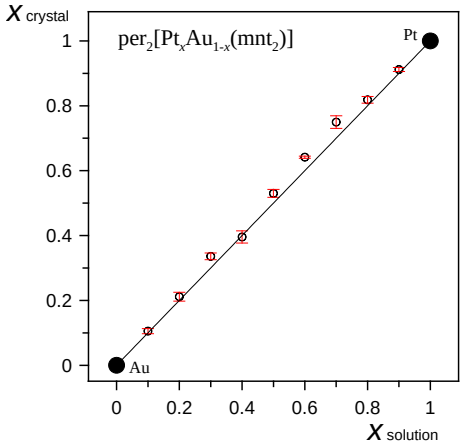

Figure 1. Pt and Au concentration of crystals $(Per)_2[Pt_x\text{-}Au_{(1-x)}(mnt)_2]$ versus growth solution concentration. The line represents a linear relation with equal solid and liquid concentrations.

The isostructural nature of the Au and Pt compounds, space group $P2_1/n$, and the close similarity of lattice and structural parameters, are further confirmed by single crystal X-ray diffraction of pure Au and Pt compounds performed in this work, which enabled a crystal structure refinement with significantly higher quality than the original data published more than 30 years ago. Crystal data are summarized in Table 1. However, as further denoted by the electrical transport properties described below, for the range of composition from x = 0.45 to 0.95, all preparations lead only to β-phase crystals and no crystals of the α-phase could be obtained. The structure of the β-polymorph in spite of its disorder nature could be further enlightened by X-ray diffraction in very small single crystals using synchrotron radiation.

Table 1. Crystal and structural refinement data for $(Per)_2[M(mnt)_2]$ compounds.

Compound	β-$(Per)_2[Pt(mnt)_2]$	α-$(Per)_2[Pt(mnt)_2]$	α-$(Per)_2[Au(mnt)_2]$
Sp.Gr.	P-1	$P2_1/n$	$P2_1/n$
a/Å	4.0105(3)	16.4258(3)	16.5632(9)
b/Å	15.2221(11)	4.1733(1)	4.1342(2)
c/Å	20.3352(13)	26.6028(4)	26.5226(12)
α/°	78.481(4)	90.0	90.0
β/°	88.200(5)	95.053(1)	94.990(3)
γ/°	86.334(5)	90.0	90.0
V/Å^3	1213.71(17)	1816.53(6)	1809.27(16)
Z, D_{calc} (Mg/m^3)	1, 1.253 [1]	2, 1.792	2, 1.802
R_1/R_w [$I > 2\sigma(I)$]	0.0775/0.1834	0.0191/0.0416	0.0694/0.1135
T/K	150(2)	150(2)	150(2)
CCDC [2]	1545581	1545582	1545583

[1] Taking into account disordered molecules in the structure for Z = 1.333, D_{calc} = 1.783. [2] Cambridge Crystallographic Data Centre reference number.

2.1. Crystal Structure

The structural refinements confirmed that compounds α-$(Per)_2[Au(mnt)_2]$ and α-$(Per)_2[Pt(mnt)_2]$ are isostructural, as previously reported [10,12], belonging to the $P2_1/n$ group with very similar lattice parameters (Table 1). The main peculiarity of these compounds is the existence of two segregated perylene and $[M(mnt)_2]$ stacks along the *b*-axis, as shown in Figure 2 for the Pt compound. There are only very small differences in the crystalline structure of these compounds with anions of identical dimensions, therefore making possible the growth of the solid solutions in the entire range of composition without any major structural changes expected.

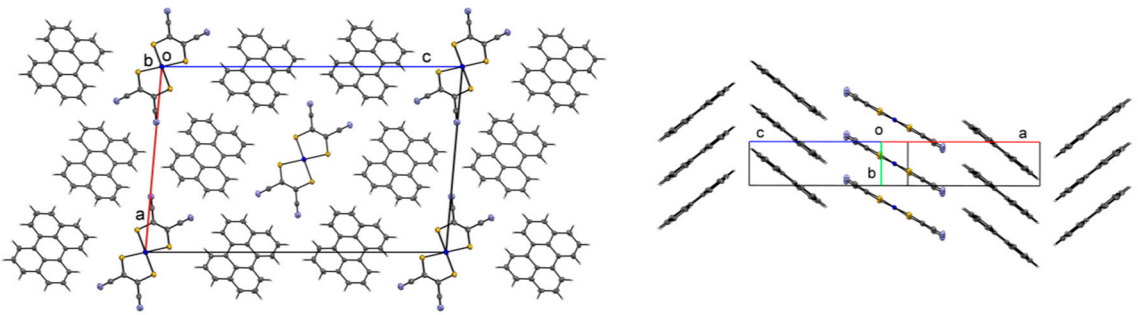

(**a**) (**b**)

Figure 2. Crystal structure of α-$(Per)_2[Pt(mnt)_2]$: (**a**) view along the *b*-axis, where segregated Per and $[Pt(mnt)_2]$ stacks can be seen. Each $[Pt(mnt)_2]$ stack is surrounded by six Per stacks, and each donor stack has three Per and three $[Pt(mnt)_2]$ stacks as first neighbors; (**b**) Partial view perpendicular to the stacking *b*-axis of parallel donor and acceptor stacks.

Besides the α-type structure summarized above, the single crystals studied by X-ray diffraction revealed also the occurrence of β-polymorphs, as first reported in the M = Ni and Cu compounds [7], and later observed in other compounds of this family with undimerised anions, namely for M = Pd [13,14] and Pt [15]. This β-polymorph is characterized by entirely different lattice parameters (Table 1) with a smaller cell volume ~1220 $Å^3$. This volume is too small to accommodate all the molecular units expected for $Z = 2$ as in the α-phases, which have cell volumes of the order of ~1840 $Å^3$, and it rather corresponds to $Z = 1.33$ assuming a similar density, denoting a disordered structure where at least one of the cell parameters should be a multiple. The disordered nature of the structure is also indicated by the presence of strong and temperature-independent diffuse scattering planes at $\pm na^*/6$, with $n = 1$, 2, and 3, as shown in Figure 3d) obtained with synchrotron radiation, indicating that the repeat unit along *a* is six-fold (~25 Å), as previously observed in the Ni and Cu compounds [7].

A full/clear structural refinement of the disordered β-phases could not be obtained. However, using diffraction data collected from a small Pt single crystal, it was possible to devise a structure containing ordered segregated donors and anion stacks along *a*, which alternated along *c*, with disordered layers. The disorder of these layers could not be satisfactorily modeled, but seemed to consist mainly in perylene molecules in two possible positions (50% occupation factors), regularly stacked along *a*.

The ordered stacks presented perylene and $[Pt(mnt)_2]$ molecules tilted towards the stacking axis in the same orientation at variance with the alternated tilting of the α-phase, and with respective interplane distances of 3.270(6) Å and 3.521(4) Å . The overlap mode was virtually identical to that observed in the α-phase where these distances are 3.287(3) and 3.609(2) Å, respectively. The disordered perylene molecules had a tilting angle and overlap mode identical to the ordered ones, and the disordered layer contained additional electron density (in voids of $V = 23{,}723$ $Å^3$, corresponding to 19.5% of unit cell volume), corresponding to additional perylene and $[Pt(mnt)_2]$ units, the positions of which could not be modelized. It is worth mentioning that the six-folding of the lattice parameter *a*

may correspond to two [Pt(mnt)$_2$] units and four perylene units in a packing pattern that repeats every 6*a* but with no coherence in the *b*,*c* plane.

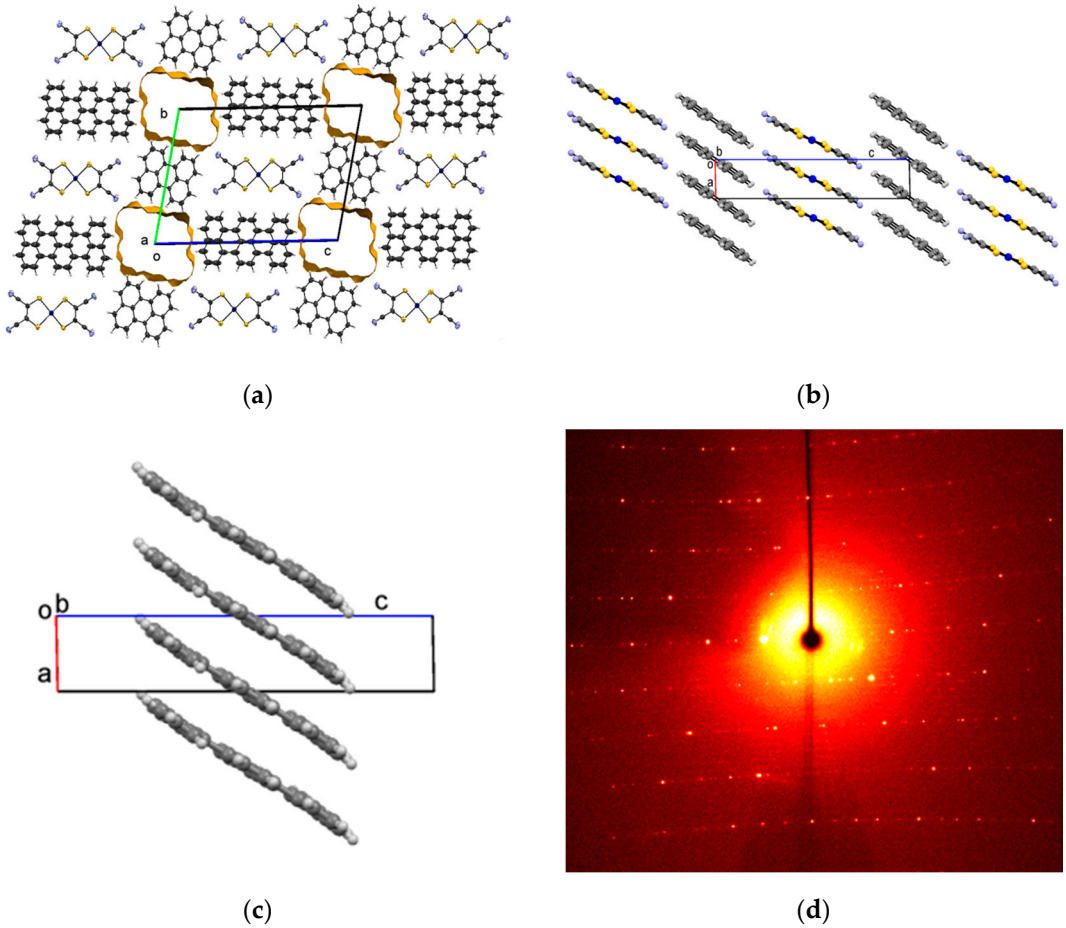

Figure 3. (**a**) Crystal structure of β-(Per)$_2$[Pt(mnt)$_2$] viewed along the stacking *a*-axis, with ordered layers of segregated perylene and [Pt(mnt)$_2$] stacks, alternating with disordered layers, in which only perylene molecules in two possible positions (50% occupation factors) could be devised; (**b**) Partial view along *b* of an ordered layer with parallel donor and acceptor stacks; (**c**) Partial view along *b* of a disordered stack of perylene molecules; (**d**) Diffraction pattern of β-(Per)$_2$[Pt(mnt)$_2$] crystal (mochromatic synchrotron radiation, fixed film fixed crystal) showing diffuse scattering planes at $\pm na^*/6$ (vertical axis).

2.2. Electrical Transport Properties—Conductivity and Thermoelectric Power

The results of the electrical transport properties measurements of (Per)$_2$[Pt$_x$-Au$_{(1-x)}$(mnt)$_2$] crystal are shown in Figure 4. The electrical resistivity ρ of the pure Pt and Au compounds closely followed the previously published results for the α-phases [16,17], with room temperature values of circa 900 S/cm (700–1200), and a clear metallic regime down to metal insulator (Peierls) transitions at 8.1 and 12.4 K respectively, which are seen by well-defined maxima in the derivative dln ρ/d(1/T). The crystals with increasing concentration in Pt, up to x = 0.40 showed a behavior comparable to that of the pure Au compound (Figure 4). There was a small sample dependence of both the sharpness of the transition and its temperature, typically ±0.1 K, which is ascribed to sample quality variations. In spite of these variations, it is clear that upon increasing Pt concentration there is first a sensible decrease of the metal-to-insulator transition from 12.2 K for x = 0 to 9.7 K for x = 0.1, followed by a much slower decrease for higher concentrations (Table 2). For x = 0.5 to 0.95, an entirely different regime of the electrical conductivity is observed; the room temperature conductivities are much smaller

(~40–60 S/cm) with a thermally-activated regime in the entire temperature range, identical to that previously described in β-phases [7,13,15]. For x = 0.98, a α-type behavior is recovered in samples from some batches, while other batches still present the β-type behavior.

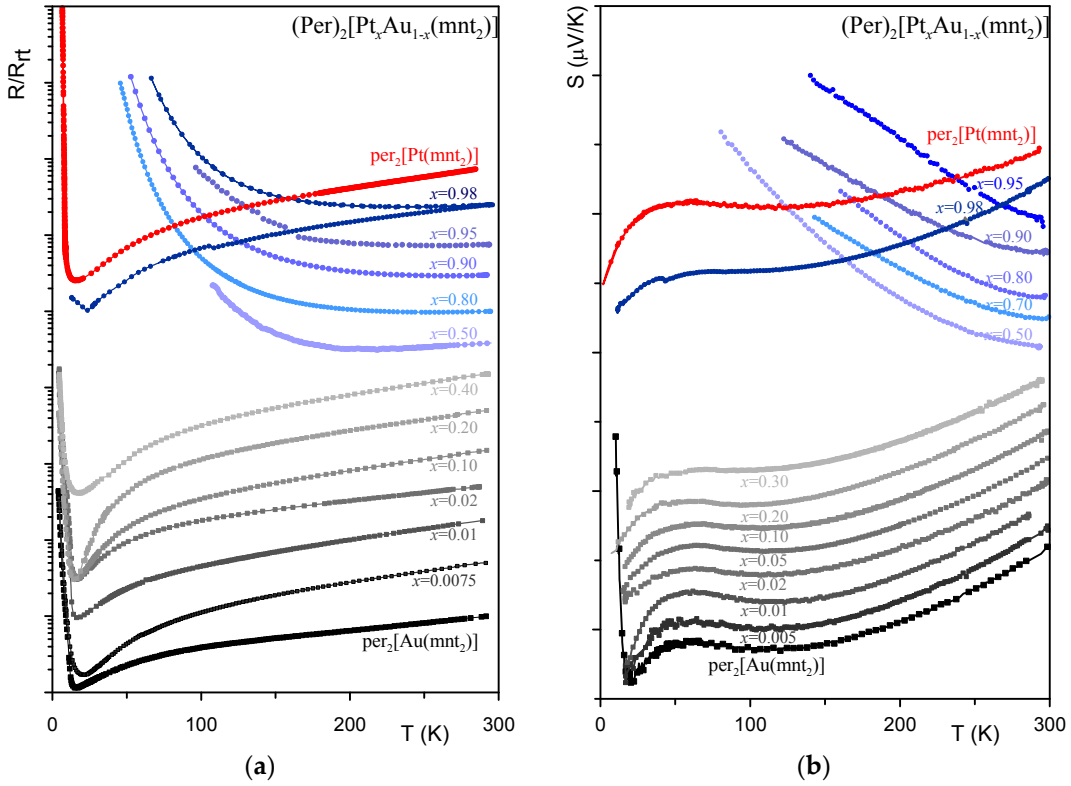

Figure 4. Electrical transport properties of (Per)$_2$[Pt$_x$-Au$_{(1-x)}$(mnt)$_2$] single crystals with composition values indicated as a function of temperature, T: (**a**) Electrical resistivity, R, plotted as ratio to the room temperature (Rrt) value; (**b**) Absolute thermoelectric power (values for increasing x are off-set by 5 μV/K at room temperature for each composition).

Table 2. Metal-to-insulator transition temperatures, $\mathbf{T_{MI}}$, of (Per)$_2$[Pt$_x$Au$_{1-x}$(mnt)$_2$] crystals as defined by maxima in the derivative of the resistivity, dln ρ/d(1/T).

x	T_{MI} (K)
0.0	12.4
0.0075	12.3
0.01	12.2
0.02	11.8
0.05	10.8
0.1	9.7
0.2	9.6
0.4	9.1
0.5	-
0.8	-
0.9	-
0.95	-
0.98 (β)	-
0.98 (α)	8.7
1.0	8.1

The thermoelectric power results (Figure 4b) also reveal the existence of two different behaviors of the samples depending on the composition, confirming the two phases denoted by resistivity measurements. For platinum concentrations up to $x = 0.40$, the thermopower exhibited a behavior similar to that of the pure Au compound, with room temperature values of the order of ~40 μV/K decreasing upon cooling in a fashion typical of a metal, until the metal-to-insulator transition was reached. For Pt concentrations x between 0.50 and 0.95, the temperature dependence of the thermopower was clearly distinct, with room temperature values of ~35 μV/K, which increased upon cooling approximately as $1/T$ in a semiconducting behavior similar to that of the β-phases of these compounds with M = Ni, Cu and Pd [7,13,15]. For high Pt concentrations with $x = 0.98$, the temperature dependence of the thermoelectric power showed again a behavior similar to that of the α-phase of the pure Pt compound, which is also almost identical to that of the Au compound. The thermoelectric power of the α-phase crystals in the high temperature range, where a linear temperature dependence was followed, is consistent with the behavior expected for a ¾-filled band 1D system. Within the tight-binding approximation, and neglecting energy dependence of the scattering time, the thermoelectric power S of an uncorrelated 1D system is expected to follow the equation [18]:

$$S = -\frac{\pi^2 k_B^2 T}{6\,|e||t|}\left[\frac{\cos(\pi\rho/2)}{\sin^2(\pi\rho/2)}\right] \quad (1)$$

where t is the transfer integral between next neighboring molecules, and ρ is the number of electrons per molecule (3/2). These approximations using the high temperature S data ($T > 100$ K) predict a bandwidth $4t = 0.58$ eV for these α-phase alloys, as for the pure compounds. This is overall in very good agreement with the values of $t = 0.143$ eV estimated from plasma frequency in reflectance [19], $t = 0.149$ eV from magnetoresistance [20,21] and $t \approx 0.148$ eV from quantum chemistry calculations under the extended Huckel approximation [22].

The semiconducting properties of the β-phases can be understood in view of the observed structural disorder. In the ordered layers of the β-phase, the regular stacking of the donors with same type of overlap and intermolecular distances comparable to those of the α-phase could lead to a similar metallic behaviour associated with an identical ¾-filled band, highly anisotropic quasi-1D system. However, the disordered layers impose an external random potential that, in this extremely anisotropic quasi-1D system, can effectively localize the electronic states.

2.3. Magnetic Susceptibility

The results of the paramagnetic susceptibility measurements of $(Per)_2[Pt_x\text{-}Au_{(1-x)}(mnt)_2]$ are shown in Figure 5. The pure Au sample, where the anions are diamagnetic, had a small Pauli-like contribution due to conduction electrons of 2.2×10^{-4} emu/mol at room temperature, which had a small decrease upon cooling and vanished at the metal-to-insulator transition, as previously reported [23] and comparable to the α-phase of the Cu compound, also with diamagnetic anions [24]. The pure Pt sample, where the anions were paramagnetic, presented a much larger paramagnetic susceptibility that in addition to a small Pauli-like contribution identical to that of the Au compound, was ascribed essentially to the paramagnetic $[Pt(mnt)_2]^-$ anions, which behaved as a chain of antiferromagnetically (AFM) coupled $S = 1/2$ spins. The maximum of paramagnetic susceptibility at ~25 K was indicative of antiferromagnetic coupling of the spins along the chains, and indeed magnetic susceptibility above the metal-to-insulator transition temperature at 8.1 K can be fairly well adjusted by the 1D Heisenberg linear chain model by Bonner-Fisher [25] with an AFM exchange interaction of $J/k_B = -15.5$ K [23]. The large paramagnetic susceptibility of the pure Pt compound experienced a sharp decrease below 8.1 K as a consequence of a spin-Peierls transition (dimerization of the anionic chains), which took place at the same temperature as the metal-to-insulator transition [26].

The main feature in the magnetic susceptibility of the solid solutions $(Per)_2[Pt_x\text{-}Au_{(1-x)}(mnt)_2]$ was that upon increasing x, the presence of paramagnetic centers in the anionic chains, gave rise to

an increasing Curie-type contribution to the paramagnetism, proportional to the Pt concentration, which soon dominated over the small Pauli-like contribution of the conducting perylene stacks. At the other extreme range of concentrations, for large x, the incorporation of diamagnetic centers in the $[Pt(mnt)_2]^-$ chains soon destroyed the spin-Peierls transition as theoretically predicted [27]. For x = 0.98, two types of samples were obtained, as previously denoted by transport measurements, one of α- and another of β-polymorph. The one corresponding to the α-phase (inset Figure 5c)) still showed a maximum of susceptibility at ~25 K and a drop of susceptibility at 8 K, although with an increased Curie tail. This effect is comparable to that experimentally observed in other spin-Peierls systems upon incorporation of non-magnetic impurities or defects, either organic systems such as p-CyDOV [28] or inorganic compounds such as $CuGeO_3$ [29]. The study of this spin-Peierls transition with larger concentrations of diamagnetic impurities was not possible in this system due to formation of β-polymorph.

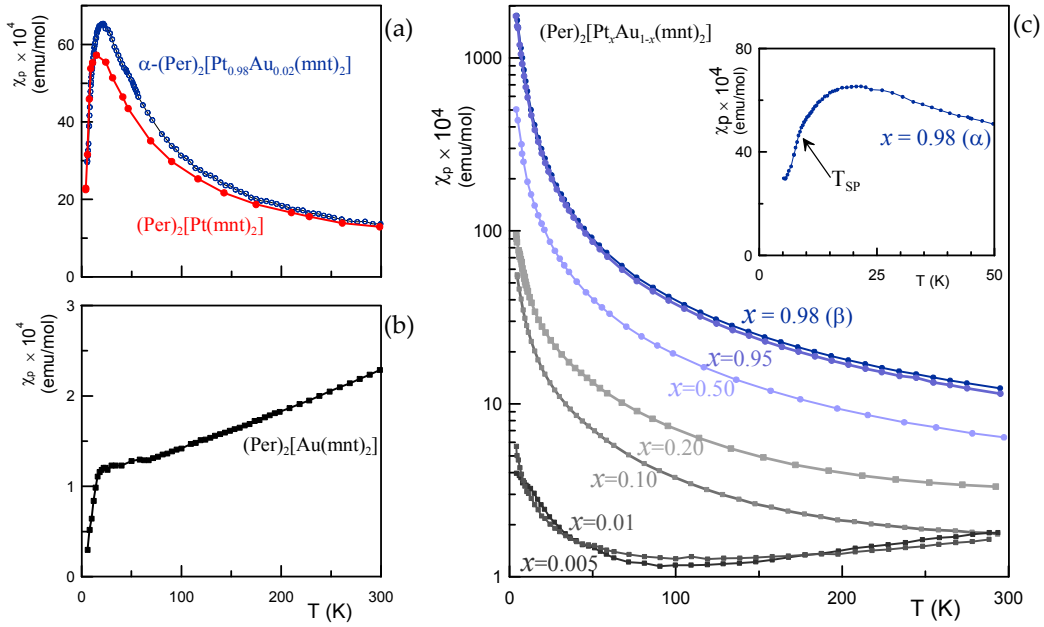

Figure 5. Paramagnetic susceptibility, χ_P, of $(Per)_2[Pt_xAu_{(1-x)}(mnt)_2]$ with composition x indicated, as a function of temperature, T. (**a**) Pt compound and x = 0.98, α-phase; (**b**) Au compound; (**c**) $0.005 \leq x \leq 0.95$ and 0.98, β-phase. The inset shows the behavior of a α-phase sample with x = 0.98.

The paramagnetic susceptibility of $(Per)_2[Pt_x\text{-}Au_{(1-x)}(mnt)_2]$ could result from donor and acceptor contributions. For the α-phase, the donor contribution, due to the delocalized conduction electrons in the perylene stacks, was expected to be identical to that of the pure Au compound. The remaining contribution of the paramagnetic $[Pt(mnt)_2]$ anions could therefore be deduced from the total paramagnetic susceptibility after subtraction of the small Pauli-like contribution of the pure Au compound. This last contribution in samples with x up to 0.95 and 0.98 of β-phase was found to follow above 50 K a Curie–Weiss law with small Weiss constants (<5 K) and Curie constant C close to that that expected for $S = 1/2$ spins with $g \approx 2.0$ (C = 0.375 emu K/mole), with no difference between α and β phases, as shown in Figure 6. A significant deviation was however observed for x = 0.98 of α-phase, which approached the behavior of the pure Pt compound.

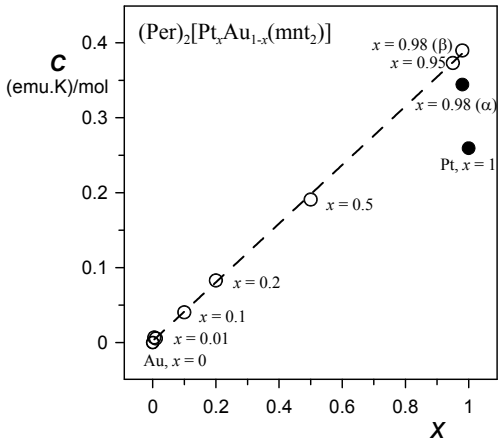

Figure 6. Curie constant, C, of the [Pt(mnt)$_2$] contribution to the paramagnetic susceptibility of (Per)$_2$[Pt$_x$-Au$_{(1-x)}$(mnt)$_2$] as a function of the composition x.

3. Materials and Methods

(Per)$_2$[Au$_{1-x}$Pt$_x$(mnt)$_2$] single crystals were obtained by electrocrystallization from dichloromethane solutions of perylene (~1.4 × 10^{-2} M) and variable relative amounts of the gold and platinum complexes as tetrabutylammonium salts (total anion concentration ~7 × 10^{-3} M) under general conditions that have been previously optimized and described in detail [11]. Special care was taken in the purification of the compounds and solvents used. Perylene (Sigma, St. Louis, MO, USA) was purified by multiple recrystallization and silica and alumina chromatography [30], followed by gradient sublimation under reduced pressure at ~110 °C. The tetrabutylammonium salts of gold and platinum were synthesized as described [31,32] and recrystallized several times from acetone under argon atmosphere. Dichloromethane was distilled, dried and passed through a column of activated alumina just before use. Galvanostatic conditions with current densities in the range of 5–20 μA/cm^2 were employed using platinum wire electrodes and two compartment cells sealed under argon. The best crystals were obtained by using a slightly increasing current over time, with an initial current of 1 μA and an increase of 1 μA every two days. The crystals were collected after 10 days and generally appeared as small black shining needles.

SEM–EDS microanalysis of the crystals were performed using a JEOL JSM 6301F microscope at CEMUP. The Au:Pt concentration ratio was estimated from the L-lines of the metals, while the K-line of sulfur was used as a control element of the analysis. Four spectra were obtained: a global spectrum in one area containing a cluster of crystals, and three others along a well-defined face of selected crystals. The typical dispersion of Pt concentration x were ±0.01. The results were found reproducible in different crystals from the same batch.

Single crystal X-ray diffraction experiments in α-(Per)$_2$[M(mnt)$_2$] crystals with M = Au and Pt and β-(Per)$_2$[Pt(mnt)$_2$] were performed with a Bruker APEX II CCD detector diffractometer, using graphite monochromated MoK$_\alpha$ radiation (λ = 0.71073 Å), in the φ and ω scans mode. A semi-empirical absorption correction was carried out using SADABS [33]. Data collection, cell refinement, and data reduction were done with the SMART and SAINT programs [34]. In the case of β-(Per)$_2$[Pt(mnt)$_2$], X-ray diffraction was also performed on a very small single crystal on a heavy-duty diffractometer at the Materials Science Beamline ID11 (λ = 0.29520 Å, ESRF, Grenoble, France) using a Frelon2K CCD detector. After conversion of the frame file format, the data were indexed using SMART, integrated with SAINT and corrected for absorption using SADABS. The structures were solved by direct methods using SIR97 [35] and refined by full matrix least-squares methods using the program SHELXL97 [36] and the winGX software package [37]. Non-hydrogen atoms were refined with anisotropic thermal parameters, whereas H atoms were placed in idealized positions and allowed to refine while riding on the parent C atom. Molecular graphics were prepared using mercury [38].

Electrical conductivity measurement in the range 4 K–300 K were performed in a helium cryostat along the long axis (*b*-axis of α-phase, *a*-axis in β-phase) using an in-line four-probe configuration,

with a current of ~1 μA of frequency (77 Hz), and the voltage drop measured by a lock-in amplifier. Contacts were made to four Au pads evaporated on each crystal, connected through colloidal platinum paint to four gold wire probes (25 μm diameter). Special care was taken to ensure low unnested/nested voltages ratios, as defined by Schaffer [39].

The thermoelectric power was also measured along the needle axis of the crystals by a slow AC technique using high purity gold wires (99.99+% Goodfellow Metals) in a cell [40] similar to the one described by Chaikin [41] placed in a closed-cycle He cryostat and operated under computer control [42]. Sample voltage was measured by a Kethley 181 nanovoltmeter. The thermal gradients were measured by a previously calibrated Au (0.07% Fe)-chromel thermocouple and a Kethley 181 nanovoltmeter, and were kept below 1 K. The sample temperature was measured by an identical Au (0.07% Fe)-chromel thermocouple. Absolute thermoelectric power was calculated after correction for the absolute thermoelectric power of gold leads using the data of Huebner [43].

Magnetic susceptibility was measured in the range 5–300 K using a Faraday system (Oxford Instruments, Oxford, UK) with a 7 T superconducting magnet. Polycrystalline samples (~5–10 mg) were placed in thin-wall Teflon buckets, previously measured. The magnetic fields used were in the range of 2 to 5 T, and the force was measured with a microbalance (Sartorius S3D-V, Goettingen, Germany) applying forward and reverse gradients of 5 T/m. Under these conditions, the magnetization was found to be proportional to the applied magnetic field. Paramagnetic molar susceptibility was obtained after a correction for the diamagnetic contribution estimated from tabulated Pascal constants at 4.2×10^{-4} emu/mol.

4. Conclusions

The results concerning the evolution of the transition temperature and type of ground states as a function of the composition of the alloys $(Per)_2[Pt_x\text{-}Au_{(1-x)}(mnt)_2]$ are summarised in Figure 7. At the low Pt concentration range, the metallic systems at high temperatures underwent a Peierls transition towards a Charge Density Wave (CDW) ground state at slightly decreasing temperatures in the range 12 K to 8 K and had an increasing Curie–Weiss component of the paramagnetic susceptibility proportional to the Pt content. At the extreme range of high Pt content, the CDW ground state of the donor stacks, which coexisted with a spin-Peierls ground state in the anionic chains for the pure Pt compound, was still present at $x = 0.98$. The effect of higher concentrations of diamagnetic impurities in the magnetic chains could not be probed since in the range $x = 0.50$ to 0.95, only β-phase crystals could be obtained. The semiconducting properties of the β-phase are a consequence of localization induced by the structural disorder.

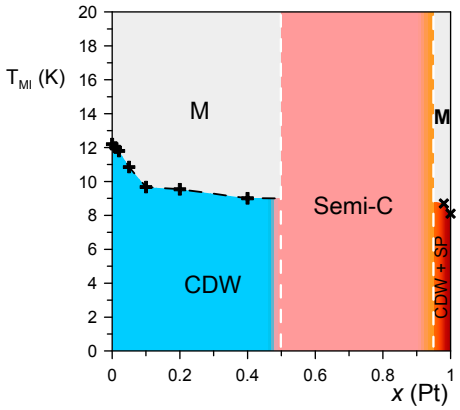

Figure 7. Phase diagram of the $(Per)_2[Pt_x\text{-}Au_{(1-x)}(mnt)_2]$ system. At left, for α-phase, it occurred a Peierls transition from a metal (M) towards a Charge Density Wave (CDW) ground state with a Curie–Weiss behaviour of the anions. At the extreme right in the α-phase, the CDW ground state of the donor stacks coexisted with a spin-Peierls (SP) ground state in the anionic chains. The spin-Peierls ground state was not suppressed by small concentrations (up to ~2%) of diamagnetic impurities. In the range x = 0.50 to 0.95, only semiconducting β-phase crystals could be obtained.

Acknowledgments: This work was partially supported by FCT (Portugal) through contracts UID/EEA/50008/2013, PTDC FIS/113500/2009 and UID/Multi/04349/2013.

Author Contributions: R.T.H. and M.A. conceived and designed the experiments and supervised the overall work; M.M. and M.L.A. prepared the samples; M.M., R.T.H. and G.B. performed electrical and magnetic meas44urements; I.C.S. performed the X-ray diffraction experiments and structure refinement; Data were analyzed by all authors; M.A. and M.M. wrote the paper with contributions from all other authors.

Conflicts of Interest: The authors declare no conflict of interest. The funding sponsors had no role in the design of the study; in the collection, analyses, or interpretation of data; in the writing of the manuscript, and in the decision to publish the results.

References

1. Alcácer, L.; Maki, A. Electrically Conducting Metal Dithiolate-Perylene Complexes. *J. Phys. Chem.* **1974**, *78*, 215–217. [CrossRef]
2. Alcácer, L.; Maki, A.H. Magnetic Properties of Some Electrically Conducting Perylene-Metal Dithiolate Complexes. *J. Phys. Chem.* **1976**, *80*, 1912–1916. [CrossRef]
3. Almeida, M.; Gama, V.; Henriques, R.T.; Alcácer, L. Molecular Solids with Organic Conducting Chains and Inorganic Magnetic Chains: The $(Per)_2M(mnt)_2$ Family (M = Ni, Cu, Pd, Pt, Au, Fe and Co). In *Inorganic and Organometallic Polymers with Special Properties*; Laine, R.M., Ed.; Kluwer Academic Publishers: Dordrecht, The Netherlands, 1992; pp. 163–177.
4. Almeida, M.; Henriques, R.T. Perylene Based Conductors. In *Handbook of Organic Conductive Molecules and Polymers Volume 1 "Charge Transfer Salts, Fullerenes and Photoconductors"*; Nalva, H.S., Ed.; John Wiley & Sons Ltd.: Chichester, UK, 1997; pp. 87–149.
5. Gama, V.; Henriques, R.T.; Bonfait, G.; Almeida, M.; Ravy, S.; Pouget, J.P.; Alcacer, L. The interplay between conduction electrons and chains of localized spins in the molecular metals $(Per)_2M(mnt)_2$, M = Au, Pt, Pd, Ni, Cu, Co and Fe. *Mol. Cryst. Liq. Cryst.* **1993**, *234*, 171–178. [CrossRef]
6. Pouget, J.-P.; Foury-Leylekian, P.; Almeida, M. Peierls and spin-Peierls instabilities in the $Per_2[M(mnt)_2]$ series of one-dimensional organic conductors; experimental realization of a 1D Kondo lattice for M = Pd, Ni and Pt. *Magnetocghemistry* **2017**, *3*, 13. [CrossRef]
7. Gama, V.; Almeida, M.; Henriques, R.T.; Santos, I.C.; Domingos, A.; Ravy, S.; Pouget, J.P. Low Dimensional Molecular Conductors $(Per)_2M(mnt)_2$, M = Cu and Ni: Low and High Conductivity Phases. *J. Phys. Chem.* **1991**, *95*, 4263–4267. [CrossRef]
8. Monchi, K.; Poirier, M.; Bourbonnais, C.; Matos, M.J.; Henriques, R.T. The Peierls transition in $Per_2[Au_xPt_{1-x}(mnt)_2]$: Pair-breaking field effects. *Synth. Met.* **1999**, *103*, 2228–2231. [CrossRef]
9. Matos, M.J.; Gama, V.; Bonfait, G.; Henriques, R.T. Magnetic and transport properties of the alloys $(Perylene)_2[Au_{1-x}Pt_x(mnt)_2]$. *Synth. Met.* **1993**, *56*, 1858–1863. [CrossRef]
10. Alcácer, L.; Novais, H.; Pedroso, F. Synthesis, structure and preliminary results on electrical and magnetic properties of $(Perylene)_2[Pt(mnt)_2]$. *Solid State Commun.* **1980**, *35*, 945–949. [CrossRef]
11. Afonso, M.L.; Silva, R.A.; Matos, M.; Henriques, R.T.; Almeida, M. Electrocrystallisation of $(perylene)_2[M(mnt)_2]$ salts. *Phys. Status Solidi* **2012**, *9*, 1123–1126. [CrossRef]
12. Domingos, A.; Henriques, R.T.; Gama, V.; Almeida, M. Crystalline structure/transport properties relationship in the $(perylene)_2M(mnt)_2$ family (M = Au, Pd, Pt, Ni). *Synth. Met.* **1988**, *27*, 411–416. [CrossRef]
13. Afonso, M.L.; Silva, R.A.; Matos, M.; Lopes, E.B.; Coutinho, J.T.; Pereira, L.C.J.; Henriques, R.T.; Almeida, M. Growth of $(Perylene)_2[Pd(mnt)_2]$ crystals. *J. Cryst. Growth* **2012**, *340*, 56–60. [CrossRef]
14. Afonso, M.L.; Silva, R.A.; Pereira, L.C.; Coutinho, J.T.; Freitas, R.R.; Lopes, E.B.; Matos, M.; Henriques, R.T.; Viana, A.; Almeida, M. Electrocrystallisation of $(Per)_2[Pd(mnt)_2]$. *Phys. Status Solidi* **2012**, *9*, 1131–1133. [CrossRef]
15. Henriques, R.T.; Sousa, I.; Dias, J.C.; Lopes, E.B.; Almeida, M.; Matos, M. Growth of High Quality $Per_2M(mnt)_2$ Single Crystals; Evidence of β-Phase in $Per_2Pt(mnt)_2$. *J. Low Temp. Phys.* **2006**, *142*, 409–412. [CrossRef]
16. Bonfait, G.; Matos, M.J.; Henriques, R.T.; Almeida, M. The Peierls transition under high magnetic field. *Physica B* **1995**, *211*, 297–299. [CrossRef]

17. Bonfait, G.; Lopes, E.B.; Matos, M.J.; Henriques, R.T.; Almeida, M. Magnetic field dependence of the metal-insulator transition in $(PER)_2Pt(mnt)_2$ and $(PER)_2Au(mnt)_2$. *Solid State Commun.* **1991**, *80*, 391–394. [CrossRef]
18. Kwak, J.F.; Beni, G.; Chaikin, P.M. Thermoelectric power in Hubbard-model systems with different densities: *N*-methylphenazinium-tetracyanoquinodimethane (NMP-TCNQ), and quinolinium ditetracyanoquinodimethane. *Phys. Rev.* **1976**, *13*, 641–646. [CrossRef]
19. Drichko, N.; Kaiser, S.; Shewmon, R.; Eckstein, J.; Wu, D.; Dressel, M.; Matos, M.; Henriques, R.T.; Almeida, M. Infrared investigations of the one-dimensional organic conductors $(perylene)_2M(mnt)_2$, M = Au, Pt. *Eur. Phys. J. B* **2010**, *78*, 283–289. [CrossRef]
20. Graf, D.; Choi, E.S.; Brooks, J.S.; Matos, M.; Henriques, R.T.; Almeida, M. High Magnetic Field Induced Charge Density Wave State in a Quasi-One-Dimensional Organic Conductor. *Phys. Rev. Lett.* **2004**, *93*, 076406. [CrossRef] [PubMed]
21. Graf, D.; Brooks, J.S.; Choi, E.S.; Uji, S.; Dias, J.C.; Almeida, M.; Matos, M. Suppression of a charge-density-wave ground state in high magnetic fields: Spin and orbital mechanisms. *Phys. Rev. B* **2004**, *69*, 125113. [CrossRef]
22. Canadell, E.; Almeida, M.; Brooks, J. Electronic band structure of α-$(Per)_2M(mnt)_2$ compounds. *Eur. Phys. J. B* **2004**, *42*, 453–456. [CrossRef]
23. Bourbonnais, C.; Henriques, R.T.; Wzieteck, P.; Köngeter, D.; Voiron, J.; Jérome, D. Nuclear and electronic resonance approaches to magnetic and lattice fluctuations in the two-chain family of organic compounds (perylene)2[M(S2C2(CN)2)2] (M = Pt, Au). *Phys. Rev. B* **1991**, *44*, 641–651. [CrossRef]
24. Gama, V.; Henriques, R.T.; Almeida, M.; Alcácer, L. Magnetic Properties of the Low-Dimensional Systems $(Per)_2M(mnt)_2$ (M = Cu and Ni). *J. Phys. Chem.* **1994**, *98*, 997–1001. [CrossRef]
25. Bonner, J.C.; Fisher, M.E. Linear Magnetic Chains with Anisotropic Coupling. *Phys. Rev. A* **1964**, *135*, 640–658. [CrossRef]
26. Henriques, R.T.; Alcácer, L.; Pouget, J.P.; Jérome, D. Electrical conductivity and X-ray diffuse scattering study of the family of organic conductors $(perylene)_2M(mnt)_2$, (M = Pt, Pd, Au). *J. Phys. C Solid State Phys.* **1984**, *17*, 5197–5208. [CrossRef]
27. Hansen, P.; Augier, D.; Riera, J.; Poilblanc, D. Study of impurities in spin-Peierls systems including lattice relaxation. *Phys. Rev.* **1999**, *59*, 13557. [CrossRef]
28. Jamali, J.B.; Wada, N.; Shimobe, Y.; Achiwa, N.; Kuwajima, S.; Soejima, Y.; Mukai, K. The effect of non-magnetic impurities on the spin–Peierls transition of 3-(4-cyanophenyl)-1,5-dimethyl-6-oxoverdazyl radical crystal, p-CyDOV. *Chem. Phys. Lett.* **1998**, *292*, 661–666. [CrossRef]
29. Pouget, J.P.; Ravy, S.; Schoeffel, J.P.; Dhalenne, G.; Revcolevschi, A. Spin-Peierls lattice fluctuations and disorders in $CuGeO_3$ and its solid solutions. *Eur. Phys. J. B* **2004**, *38*, 581–598. [CrossRef]
30. Sangster, R.C.; Irvine, J.W., Jr. Study of Organic Scintillators. *J. Chem. Phys.* **1956**, *24*, 670–715. [CrossRef]
31. Davison, A.; Holm, R.H. Metal Complexes Derived from cis-1,2-Dicyano-ethylene-1,2-Dithiolate and Bis-Perfluoromethyl-1,2-Dithietene. *Inorg. Synth.* **1967**, *10*, 8–26.
32. Davison, A.; Edelstein, N.; Holm, R.H.; Maki, A.H. E.s.r. Studies of Four-Coordinate Complexes of Nickel, Palladium and Platinum Related by Electron Transfer Reactions. *J. Am. Chem. Soc.* **1963**, *85*, 2029–2030. [CrossRef]
33. Sheldrick, G.M. *SADABS*; Bruker AXS Inc.: Madison, WI, USA, 2004.
34. Bruker. *SMART and SAINT*; Bruker AXS Inc.: Madison, WI, USA, 2004.
35. Altomare, A.; Burla, M.C.; Camalli, M.; Cascarano, G.L.; Giacovazzo, C.; Guagliardi, A.; Moliterni, A.G.G.; Polidori, G.; Spagna, R. SIR97: A new tool for crystal structure determination and refinement. *Appl. Crystallogr.* **1999**, *32*, 115–119. [CrossRef]
36. Sheldrick, G.M. A short history of SHELX. *Acta Crystallogr. Sect. A* **2008**, *64*, 112–122. [CrossRef] [PubMed]
37. Farrugia, L.J. WinGX and ORTEP for Windows: An update. *J. Appl. Crystallogr.* **2012**, *45*, 849–854. [CrossRef]
38. Macrae, C.F.; Bruno, I.J.; Chisholm, J.A.; Edgington, P.R.; McCabe, P.; Pidcock, E.; Rodriguez-Monge, L.; Taylor, R.; van de Streek, J.; Wood, P.A. Mercury CSD 2.0—New features for the visualization and investigation of crystal structures. *J. Appl. Cryst.* **2008**, *41*, 466–470. [CrossRef]
39. Schafer, D.E.; Wudl, F.; Thomas, G.A.; Ferraris, J.P.; Cowan, D.O. Apparent giant conductivity peaks in an anisotropic medium: TTF-TCNQ. *Solid State Commun.* **1974**, *14*, 347–351. [CrossRef]

40. Almeida, M.; Alcácer, L.; Oostra, S. Anisotropy of thermopower in *N*-methyl-*N*-ethylmorpholinium bistetracyanoquinodimethane, MEM(TCNQ)2, in the region of the high-temperature phase transitions. *Phys. Rev. B* **1984**, *30*, 2839. [CrossRef]
41. Chaikin, P.M.; Kwak, J.F. Apparatus for thermopower measurements on organic conductors. *Rev. Sci. Instrum.* **1975**, *46*, 218. [CrossRef]
42. Lopes, E.B. *Internal Report*; LNETI: Sacavém, Portugal, 1990.
43. Huebner, R.P. Thermoelectric Power of Lattice Vacancies in Gold. *Phys. Rev.* **1964**, *135*, 1281–1291. [CrossRef]